Science
AAAS

InP Nanowire Array Solar Cells Achieving 13.8% Efficiency by Exceeding the Ray Optics Limit
Jesper Wallentin *et al.*
Science **339**, 1057 (2013);
DOI: 10.1126/science.1230969

Science (print ISSN 0036-8075; online ISSN 1095-9203) is published weekly, except the last week in December, by the American Association for the Advancement of Science, 1200 New York Avenue NW, Washington, DC 20005.

between the arrival times of electrons at a beam splitter is a signature of two-particle interference, which demonstrates the possibility of generating coherent and indistinguishable single-electron wave packets with independent sources. It provides the possibility of controlled manipulation of single-electron states in quantum conductors, with applications in quantum information processing, but could also be used to fully reconstruct the wave function of a single electron (*24*, *30*) and thus quantitatively address the propagation of a single excitation propagating in a complex environment.

References and Notes

1. Y. Ji *et al.*, *Nature* **422**, 415 (2003).
2. P. Roulleau *et al.*, *Phys. Rev. Lett.* **100**, 126802 (2008).
3. M. Yamamoto *et al.*, *Nat. Nanotechnol.* **7**, 247 (2012).
4. Y. Blanter, M. Büttiker, *Phys. Rep.* **336**, 1 (2000).
5. E. Knill, R. Laflamme, G. J. Milburn, *Nature* **409**, 46 (2001).
6. A. Bertoni, P. Bordone, R. Brunetti, C. Jacoboni, S. Reggiani, *Phys. Rev. Lett.* **84**, 5912 (2000).
7. C. K. Hong, Z. Y. Ou, L. Mandel, *Phys. Rev. Lett.* **59**, 2044 (1987).
8. J. Beugnon *et al.*, *Nature* **440**, 779 (2006).
9. R. C. Liu, B. Odom, Y. Yamamoto, S. Tarucha, *Nature* **391**, 263 (1997).
10. P. Samuelsson, E. V. Sukhorukov, M. Büttiker, *Phys. Rev. Lett.* **92**, 02685 (2004).
11. I. Neder *et al.*, *Nature* **448**, 333 (2007).
12. G. Fève *et al.*, *Science* **316**, 1169 (2007).
13. M. D. Blumenthal *et al.*, *Nat. Phys.* **3**, 343 (2007).
14. C. Leicht *et al.*, *Semicond. Sci. Technol.* **26**, 055010 (2011).
15. S. Hermelin *et al.*, *Nature* **477**, 435 (2011).
16. R. P. G. McNeil *et al.*, *Nature* **477**, 439 (2011).
17. A. Mahé *et al.*, *Phys. Rev. B* **82**, 201309(R) (2010).
18. M. Albert, C. Flindt, M. Büttiker, *Phys. Rev. B* **82**, 041407(R) (2010).
19. T. Jonckheere, T. Stoll, J. Rech, T. Martin, *Phys. Rev. B* **85**, 045321 (2012).
20. F. D. Parmentier *et al.*, *Phys. Rev. B* **85**, 165438 (2012).
21. E. Bocquillon *et al.*, *Phys. Rev. Lett.* **108**, 196803 (2012).
22. M. Henny *et al.*, *Science* **284**, 296 (1999).
23. W. D. Oliver, J. Kim, R. C. Liu, Y. Yamamoto, *Science* **284**, 299 (1999).
24. C. Grenier *et al.*, *New J. Phys.* **13**, 093007 (2011).
25. T. Jonckheere, J. Rech, C. Wahl, T. Martin, *Phys. Rev. B* **86**, 125425 (2012).
26. S. Ol'khovskaya, J. Splettstoesser, M. Moskalets, M. Büttiker, *Phys. Rev. Lett.* **101**, 166802 (2008).
27. G. Fève, P. Degiovanni, T. Jolicoeur, *Phys. Rev. B* **77**, 035308 (2008).
28. M. Moskalets, P. Samuelsson, M. Büttiker, *Phys. Rev. Lett.* **100**, 086601 (2008).
29. P. Degiovanni, C. Grenier, G. Fève, *Phys. Rev. B* **80**, 241307(R) (2009).
30. G. Haack, M. Moskalets, J. Splettstoesser, M. Büttiker, *Phys. Rev. B* **84**, 081303 (2011).

Acknowledgments: This work is supported by the Agence Nationale de la Recherche grant "1shot," ANR-2010-BLANC-0412.

9 November 2012; accepted 18 December 2012
Published online 24 January 2013;
10.1126/science.1232572

InP Nanowire Array Solar Cells Achieving 13.8% Efficiency by Exceeding the Ray Optics Limit

Jesper Wallentin,[1] Nicklas Anttu,[1] Damir Asoli,[2] Maria Huffman,[2] Ingvar Åberg,[2] Martin H. Magnusson,[2] Gerald Siefer,[3] Peter Fuss-Kailuweit,[3] Frank Dimroth,[3] Bernd Witzigmann,[4] H. Q. Xu,[1,5] Lars Samuelson,[1] Knut Deppert,[1] Magnus T. Borgström[1]*

Photovoltaics based on nanowire arrays could reduce cost and materials consumption compared with planar devices but have exhibited low efficiency of light absorption and carrier collection. We fabricated a variety of millimeter-sized arrays of p-type/intrinsic/n-type (p-i-n) doped InP nanowires and found that the nanowire diameter and the length of the top n-segment were critical for cell performance. Efficiencies up to 13.8% (comparable to the record planar InP cell) were achieved by using resonant light trapping in 180-nanometer-diameter nanowires that only covered 12% of the surface. The share of sunlight converted into photocurrent (71%) was six times the limit in a simple ray optics description. Furthermore, the highest open-circuit voltage of 0.906 volt exceeds that of its planar counterpart, despite about 30 times higher surface-to-volume ratio of the nanowire cell.

Nanostructures are currently being investigated for next-generation photovoltaic (PV) architectures as a means of lowering cost (*1*) through the use of abundant materials (*2*) or to improve light trapping (*3*). Nanowire (NW) arrays could provide substantial reductions in material consumption as well as production costs for III-V-based solar cells, in part because they can be monolithically grown on low-cost substrates such as silicon (*4*). However, proof of concepts of III-V NW-based PV (*5*–*9*), have had limited efficiencies in the 3 to 5% range.

The efficiency of NW-based solar cells is often limited by light absorption, especially when the NWs have subwavelength dimensions. In a ray optics description, the maximum fraction of normally incident sunlight that could be absorbed and converted to a photocurrent is proportional to the surface coverage of the active material. However, theoretical modeling based on wave optics has predicted resonant light trapping in sub-200-nm-diameter NW arrays (*10*–*12*), which would allow bulklike photocurrent generation with just a fraction of the materials consumption. Experimental studies have been confined to NW arrays with either large-diameter wires (*13*, *14*) or high surface coverage (*9*). Another limitation is that crystal surfaces typically have a high density of defects that act as potential recombination centers, and nanostructured devices have high surface-to-volume (S/V) ratios. Surface recombination could explain the hitherto observed relatively low open-circuit voltages (V_{oc}) in NW-based PV cells (*8*, *9*).

Here, we demonstrate how these challenges can be overcome and report on a NW array solar cell with 13.8% efficiency. Although the 180-nm-diameter InP NWs only cover 12% of the surface, they deliver 83% of the photocurrent density obtained in planar InP solar cells (*15*, *16*). Furthermore, the highest V_{oc} exceeds that of the InP planar record cell (*15*, *16*), despite about 30 times higher S/V ratio in our NW-based PV cell. By using three-dimensional (3D) optical modeling, we provide insight into the origins of the high performance of our solar cells, as well as guidelines to how they further can be improved.

We chose InP not only because of its direct band gap of 1.34 eV (925 nm wavelength-equivalent), suitable for the solar spectrum but also because it allows in situ etching with HCl during NW growth to prevent short-circuiting from radial overgrowth (*17*). The InP NWs in our solar cells were epitaxially grown with an axially defined p-type/intrinsic/n-type (p-i-n) doped structure (*7*) and have a length of ~1.5 μm. We used a nanoimprint technique to arrange gold seed particles in arrays (*18*). (Fig. 1, A to C). Different sizes and array pitches of the Au seeds were used, resulting in samples with different NW diameters (130 to 190 nm) and array pitches (470 or 500 nm). To reduce reflection, we removed the metal seed particles after growth by using wet etching and defined a top contact with a silicon oxide insulating layer and a transparent conducting oxide (TCO) (*7*). Last, the 1-mm-by-1-mm cells and metal contact pads were defined with optical lithography (Fig. 1C), with each sample containing a few solar cells. Details of the samples (table S1) and their fabrication are given in the supplementary materials (*19*).

Characterization of the solar cells (Fig. 1D) revealed very good performance in comparison with other InP PV architectures (Table 1). At 1-sun

[1]Solid State Physics, Lund University, Box 118, 22100 Lund, Sweden. [2]Sol Voltaics AB, Ideon Science Park, Scheelevägen 17, 22370 Lund, Sweden. [3]Fraunhofer ISE, Heidenhofstrasse 2, D-79110 Freiburg, Germany. [4]University of Kassel, Wilhelmshoeher Allee 71, 34121, Kassel, Germany. [5]Key Laboratory for the Physics and Chemistry of Nanodevices and Department of Electronics, Peking University, Beijing 100871, China.

*To whom correspondence should be addressed. E-mail: magnus.borgstrom@ftf.lth.se

(1000 W/m^2) illumination, measured in ambient air at the Fraunhofer ISE CalLab reference setup, our best cell (from sample A) shows a conversion efficiency η = 13.8% and a photocurrent density J_{sc} = 24.6 mA/cm^2. Because our calculation of J_{sc} accounts for the full (unmetalized) cell area rather than the NW surface coverage only, it can be compared with that of the best reported planar InP cell [J_{sc} = 29.5 mA/cm^2 (*15*, *16*)] and the theoretical limit of 34.5 mA/cm^2 [assuming that each incident photon with energy above the InP band gap generates one electron-hole pair (*19*)]. Thus, our cell reaches 83% of the best reported planar J_{sc} despite covering only 12% of the surface area. Our axially defined NW solar cell outperforms similar cells based on core-shell NWs with a surface coverage of 27% (*9*), as well as several other next-generation PV architectures (Table 1).

Our results demonstrate that ray optics is not appropriate for describing the interaction of light with these subwavelength structures, because the maximum J_{sc} in the ray optics picture, 4.2 mA/cm^2 (12% of the theoretical limit, 34.5 mA/cm^2), is almost six times lower than the J_{sc} of our best cell. Alternatively, a hypothetical calculation on the single-NW level, using the NW cross-sectional area, would give a physically impossible efficiency above 100%. Thus, light that would travel between the NWs in a ray optics description was absorbed efficiently in the experimental cell.

To more accurately study the absorption of light in the NW solar cell, we used full 3D electromagnetic optical modeling (figs. S1 to S3) (*20*). The validity of our approach is confirmed by comparing the calculated absorptance spectrum of the NWs in the record cell and its measured external quantum efficiency (EQE) (Fig. 2A). The values and general trends of these two spectra agree well, although the calculated absorptance is greater than the measured EQE throughout the spectrum. This discrepancy can be attributed to the absorption modeling not taking into account any carrier losses. We also show the measured EQE of a 130-nm-diameter NW solar cell (sample D) (blue solid line in Fig. 2A) and note that the EQE increases slowly above the band gap energy (925 nm in wavelength). The relatively weak coupling leads to weak absorption of long-wavelength photons into these small-diameter NWs (*21*).

We identified two key design parameters that influence the performance of our solar cells: the NW diameter and the length of the top n-segment. We show (Fig. 2B) the calculated absorption versus NW diameter assuming a constant NW length (1.4 μm) and array pitch (470 nm). The absorption increases with increasing diameter until it saturates around 180 nm, in line with previous modeling of unprocessed NW arrays (*10*). Experimentally we also saw improvement in the measured average J_{sc} from 14.0 mA/cm^2 (sample D) to 17.4 mA/cm^2 (B) when increasing the diameter from 130 to 180 nm for the same n-segment growth time of 3 min. To reach the highest J_{sc} (sample A), we also shortened the n-segment as described below. For the 180-nm diameter, the remaining 7% of the available sunlight (red area in Fig. 2B) could in principle be captured by increasing the NW length. In this work, we chose to keep the length as constant as possible in order to investigate other parameters.

The second key design parameter is the length of the top n-segment. The 3D simulations indicate that the strongest optical generation of carriers occurs near the top of the NWs (Fig. 3A). Because of the high doping, the recombination losses in the top n-segment are expected to be high. We experimentally varied the n-segment growth time (Fig. 3B) and found that reducing the nominal n-segment length from 180 (sample B) to 60 (A) nm increased the average J_{sc} by 39%. Conversely, an increase to 360 nm (sample C) reduced the average J_{sc} by 34%. These three samples are also indicated in Fig. 2B, showing that the reduction in n-segment length actually increased J_{sc} more

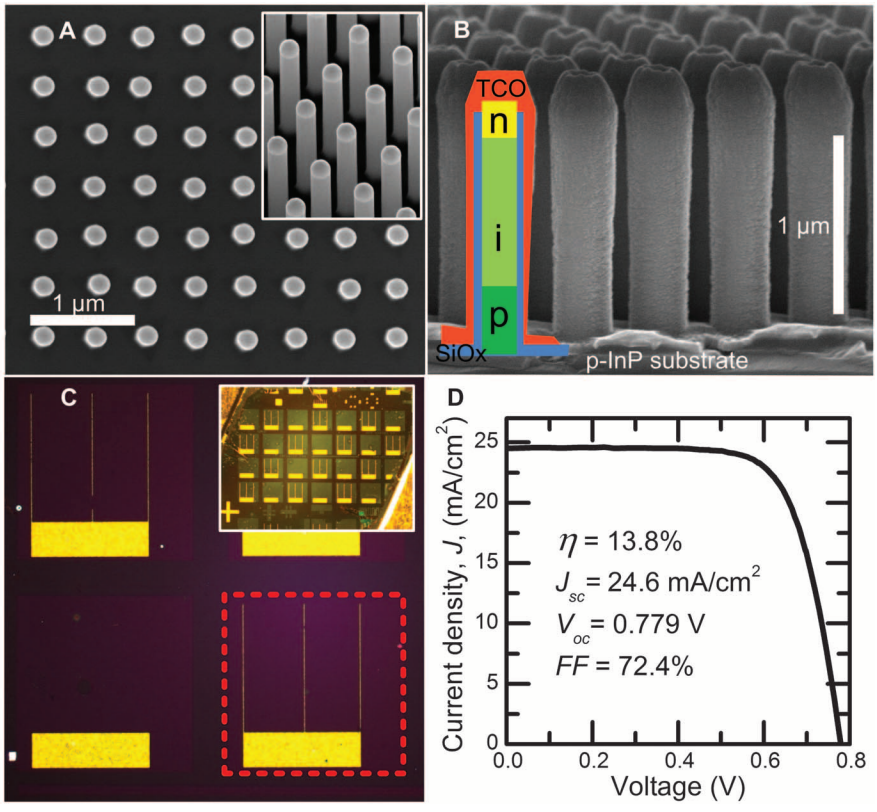

Fig. 1. Characterization of NW-array solar cells: (**A**) 0° and 30° (inset) tilt scanning electron microscopy (SEM) images of as-grown NWs with a surface coverage of 12%. (**B**) SEM image of processed NWs. The superimposed schematics illustrate the silicon oxide (SiO_x, blue), TCO (red), and the p-i-n doping layers in the NWs. (**C**) Optical microscope image of NW solar cells. The dashed red line highlights the border of a 1-mm-by-1-mm cell. (Inset) A sample with four-by-seven cells. (**D**) The 1-sun *J-V* curve for the highest-efficiency cell (sample A).

Table 1. A comparison of the performance of InP PV architectures, as well as reported efficiencies of selected next-generation PV architectures, under 1-sun illumination. The listed devices show variation in cell area and measurement conditions.

	Active area coverage (%)	Relative active volume (%)	J_{sc} (mA/cm^2)	V_{oc} (V)	Fill factor (%)	Efficiency 1 sun (%)
Axial InP NW - this work, A	12	5	24.6	0.779	72.4	13.8
Sample E	11	5	18.2	0.906	78.6	13.0
Planar InP (*15*, *16*)	100	100	29.5	0.878	85.4	22.1
Core-shell InP NW (*9*)	27	14	13.7	0.43	57	3.37
Dye-sensitized (*27*)	100		17.66	0.935	74	12.3
Organic (*16*)	100		10.08	1.53	68.5	10.6
Colloidal quantum dot (*28*)	100		20.1	0.605	58	7.0

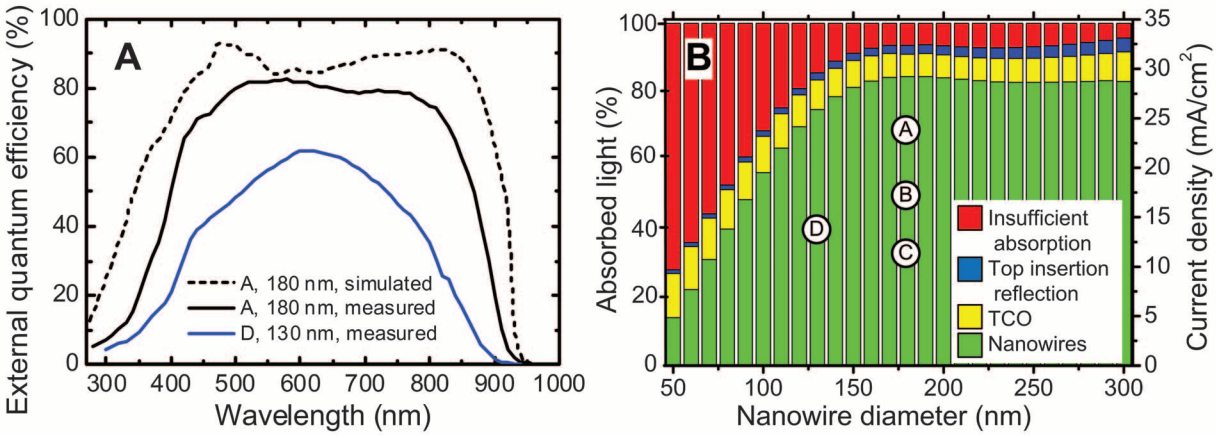

Fig. 2. Absorption in NW solar cells (**A**) Measured EQE of cells from samples A (180-nm diameter) and D (130 nm), with the simulated EQE of sample A assuming that all carriers generated in the whole NW (including the top n-segment) contribute to J_{sc}. (**B**) Simulated absorbed light as a fraction of the solar spectrum above the InP band gap and calculated J_{sc} versus NW diameter. Different optical losses are also shown (fig. S2). The markers indicate the experimentally measured average J_{sc} of samples A, B, C, and D (1-, 3-, 6-, and 3-min n-segment growth times, respectively).

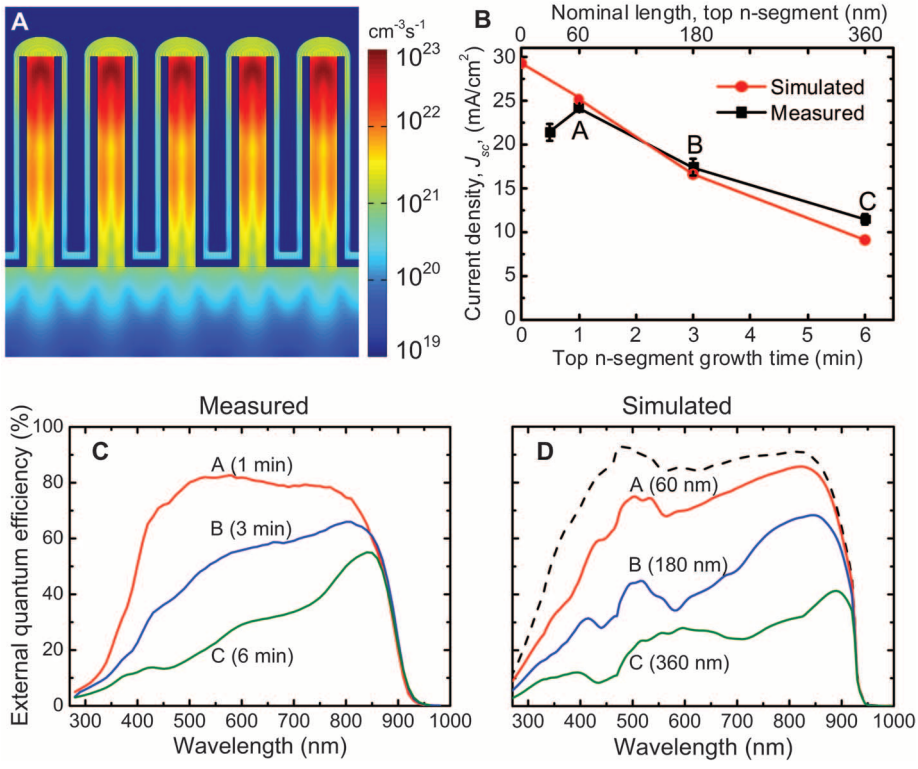

Fig. 3. Solar cell performance dependence on top n-segment length. (**A**) Simulated optical generation rate of electron-hole pairs in the *y-z* cross section of sample A for *x* polarized incident light (*19*). (**B**) Measured and simulated J_{sc} versus n-segment growth time (*19*). The error bars are one standard deviation. (**C**) Measured EQE of cells from samples A (n-segment growth time, 1 min), B (3 min), and C (6 min). (**D**) Simulated EQE of samples A (60-nm n-segment length), B (180 nm), and C (360 nm), together with the simulated EQE for sample A without losses (dashed line).

than the increase in diameter from 130 to 180 nm. With a 30-nm n-segment, the photocurrent was reduced, possibly because some slightly shorter NWs were not properly contacted.

To understand these experimental findings, we expanded our purely optical model by assuming that all carriers generated in the n-region are lost and calculated the resulting J_{sc} (Fig. 3B) and EQE (Fig. 3D). Although this simple model neglects the effects of graded doping profiles, carrier diffusion, and electrical fields, it reproduces the experimental data well. Primarily the short-wavelength light is lost, because it is most strongly absorbed at the top. We note that the modeled spectra contain sharper peaks compared with the experimental EQE (Fig. 3C). This difference probably stems from small variations in NW diameter, length position, and doping profile, which occur naturally in the experimental cells.

Next, we discuss the ability of our solar cells in transferring the photogenerated charge carriers to the contacts. The highest V_{oc} that we observed, 0.906 V, measured in sample E that has 13.0% efficiency, exceeds that of the planar InP record cell (*15*) (Table 1). In contrast, the highest-efficiency, highest-current sample, A, shows a substantially lower V_{oc}, 0.779 V. The relative variation in V_{oc} between our samples is typically greater than that for J_{sc}. Because the dimensions of the NWs in these samples are similar, we believe that this is due to variations in the contact-formation process. We therefore anticipate larger cells to show similar J_{sc} but lower V_{oc} than our best cells.

The highest V_{oc}, 0.906 V, is notable considering that the depletion region, estimated by the nominally 650-nm-long i-region, is several times longer than the NW diameter (190 nm). InP NWs have a relatively low surface-recombination velocity (*22*), with values as low as 170 cm/s reported for undoped InP NWs (*23*). Because we did not use any intentional surface passivation or high-band gap window layer, we suggest three possible origins to the high V_{oc} values observed in our NW-based solar cells in comparison to planar cells. First, the crystal structure in InP NWs is typically a mixture of wurtzite and zinc blende (*7*). Because wurtzite InP has an 80-meV higher band gap than the bulk zinc blende, this could at most produce an 80-mV increase in V_{oc} (*24*, *25*). Second, the carriers are confined to the NW cross-sectional area rather than the cell area, which means that the saturation current density, J_0, as measured by using the cell area, could be reduced by a factor of 0.12. With the formula $V_{oc} = (kT/q)\ln(J_{sc}/J_0)$ (where k is the Boltzmann constant, T is the absolute temperature, and q is the elemental charge), we can estimate this enhancement to 55 mV. Third, there could be a radial charge separation of electrons and holes, resulting from

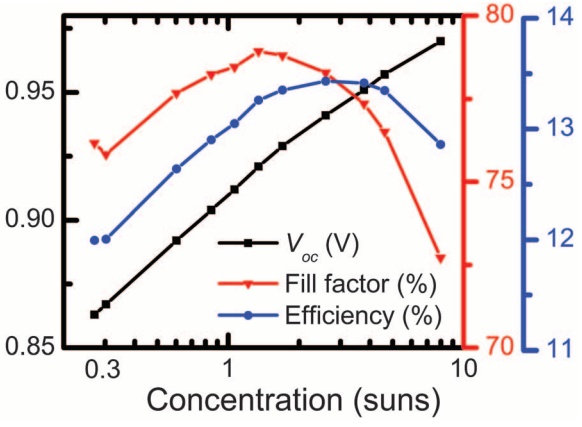

Fig. 4. Characterization of cell from sample E under concentrated illumination.

effects such as surface pinning (*26*). Additional experiments are needed to understand the high V_{oc}.

Because multijunction III-V PV is currently being deployed for concentrator PV—where large-area, low-cost optics are used to collect sunlight and focus it onto small, high-performance solar cells—we have also investigated the performance of the cell with highest V_{oc} (sample E) under concentration (Fig. 4). The V_{oc} increases logarithmically as expected up to 0.97 V. However, the fill factor decreases, which indicates a series resistance, possibly originating from the TCO or the small contact area of the NW tips. The efficiency under concentrated illumination for this cell therefore peaks at 13.4% at 2.6 suns. The angular dependence, which is important for diffuse light conditions, has not been investigated experimentally, but previous simulations have indicated weak angular dependence up to 40° (*12*).

Lastly, we assess the technical maturity of our design. We fabricated seven working cells on the same sample (average efficiency of 12.0% with standard deviation of 1.4%) and reproduced similar results in separate growth and processing batches. The best sample was stored 2 months in ambient air before the measurement, and the degradation in absolute efficiency of somewhat older samples is less than 0.5% over a period of 6 months. This design should be readily scalable to wafer-sized cells and be useful for similar optoelectronic devices such as photodetectors.

References and Notes

1. W. U. Huynh, J. J. Dittmer, A. P. Alivisatos, *Science* **295**, 2425 (2002).
2. B. O'Regan, M. Grätzel, *Nature* **353**, 737 (1991).
3. A. Polman, H. A. Atwater, *Nat. Mater.* **11**, 174 (2012).
4. T. Mårtensson *et al.*, *Nano Lett.* **4**, 1987 (2004).
5. C. Colombo, M. Heiß, M. Grätzel, A. Fontcuberta i Morral, *Appl. Phys. Lett.* **94**, 173108 (2009).
6. J. F. Wang, M. S. Gudiksen, X. Duan, Y. Cui, C. M. Lieber, *Science* **293**, 1455 (2001).
7. M. T. Borgström *et al.*, *IEEE J. Sel. Top. Quantum Electron.* **17**, 1050 (2011).
8. E. C. Garnett, M. L. Brongersma, Y. Cui, M. D. McGehee, *Annu. Rev. Mater. Res.* **41**, 269 (2011).
9. H. Goto *et al.*, *Appl Phys Express* **2**, 035004 (2009).
10. J. Kupec, R. L. Stoop, B. Witzigmann, *Opt. Express* **18**, 27589 (2010).
11. L. Hu, G. Chen, *Nano Lett.* **7**, 3249 (2007).
12. N. Anttu, H. Q. Xu, *J. Nanosci. Nanotechnol.* **10**, 7183 (2010).
13. M. D. Kelzenberg *et al.*, *Nat. Mater.* **9**, 368 (2010).
14. E. Garnett, P. D. Yang, *Nano Lett.* **10**, 1082 (2010).
15. C. J. Keavney, V. E. Haven, S. M. Vernon, in *Photovoltaic Specialists Conference, 1990, Conference Record of the Twenty First IEEE* (IEEE, Piscataway, NJ, 1990), vol. 1, pp. 141–144.
16. M. A. Green, K. Emery, Y. Hishikawa, W. Warta, E. D. Dunlop, *Prog. Photovolt. Res. Appl.* **20**, 606 (2012).
17. M. T. Borgström *et al.*, *Nano Research* **3**, 264 (2010).
18. T. Mårtensson *et al.*, *Nano Lett.* **4**, 699 (2004).
19. See supplementary materials on *Science* Online.
20. N. Anttu, H. Q. Xu, *Phys. Rev. B* **83**, 165431 (2011).
21. P. M. Wu, N. Anttu, H. Q. Xu, L. Samuelson, M. E. Pistol, *Nano Lett.* **12**, 1990 (2012).
22. S. Münch *et al.*, *Nanotechnology* **21**, 105711 (2010).
23. H. J. Joyce *et al.*, *Nano Lett.* **12**, 5325 (2012).
24. A. Mishra *et al.*, *Appl. Phys. Lett.* **91**, 263104 (2007).
25. O. J. Glembocki, H. Piller, in *Handbook of Optical Constants of Solids*, E. D. Palik, Ed. (Academic Press, Orlando, FL, 1985), pp. 503–516.
26. M. H. M. van Weert *et al.*, *Appl. Phys. Lett.* **88**, 043109 (2006).
27. A. Yella *et al.*, *Science* **334**, 629 (2011).
28. A. H. Ip *et al.*, *Nat Nano* **7**, 577 (2012).

Acknowledgments: This work was performed within the Nanometer Structure Consortium at Lund University (nmC@LU) and was supported by the Swedish Research Council (Vetenskapsrådet), by the Knut and Alice Wallenberg Foundation, by the Swedish Energy Agency, and by the European Union program AMON-RA (214814). This Report is based on a project that was funded by E.ON AG as part of the E.ON International Research Initiative. We thank M. Graczyk for nanoimprint lithography and S. Lehmann for transmission electron microscopy.

Supplementary Materials

www.sciencemag.org/cgi/content/full/science.1230969/DC1
Materials and Methods
Figs. S1 to S3
Table S1
References (*29*–*33*)

1 October 2012; accepted 17 December 2012
Published online 17 January 2013;
10.1126/science.1230969

Synchronous Change of Atmospheric CO_2 and Antarctic Temperature During the Last Deglacial Warming

F. Parrenin,[1]* V. Masson-Delmotte,[2] P. Köhler,[3] D. Raynaud,[1] D. Paillard,[2] J. Schwander,[4] C. Barbante,[5,6] A. Landais,[2] A. Wegner,[3]† J. Jouzel[2]

Understanding the role of atmospheric CO_2 during past climate changes requires clear knowledge of how it varies in time relative to temperature. Antarctic ice cores preserve highly resolved records of atmospheric CO_2 and Antarctic temperature for the past 800,000 years. Here we propose a revised relative age scale for the concentration of atmospheric CO_2 and Antarctic temperature for the last deglacial warming, using data from five Antarctic ice cores. We infer the phasing between CO_2 concentration and Antarctic temperature at four times when their trends change abruptly. We find no significant asynchrony between them, indicating that Antarctic temperature did not begin to rise hundreds of years before the concentration of atmospheric CO_2, as has been suggested by earlier studies.

Analyses of polar ice cores have shown that the concentration of atmospheric CO_2 (aCO_2) and surface air temperature are closely related and that they have risen and fallen in tandem over most of the past 800,000 years. However, whether changes of temperature occurred first and how large that lead may have been have been topics of considerable controversy. The most highly resolved aCO_2 record during the last deglacial warming, Termination I (TI), is from the European Project for Ice Coring in Antarctica (EPICA) Dome C (EDC) ice core (*1*, *2*). In this record, aCO_2 appears to lag local Antarctic temperature (AT) by 800 ± 600 years at the onset of TI, in agreement with an earlier study on the Vostok and Taylor Dome ice cores, which identified a lag of 600 ± 400 years at the end of the

[1]Laboratoire de Glaciologie et Géophysique de l'Environnement (CNRS/UJF), Grenoble, France. [2]Laboratoire des Sciences du Climat et de l'Environnement (CEA/CNRS/UVSQ-IPSL), Gif-sur-Yvette, France. [3]Alfred Wegener Institute for Polar and Marine Research, Bremerhaven, Germany. [4]Physics Institute, University of Bern, Bern, Switzerland. [5]Department of Environmental Sciences, University of Venice, Venice, Italy. [6]Institute for the Dynamics of Environmental Processes–CNR, University of Venice, Venice, Italy.

*Corresponding author. E-mail: parrenin@ujf-grenoble.fr
†Present address: Byrd Polar Research Center, Ohio State University, Columbus, OH, USA.